International Journal of Advanced Engineering Research and Science (IJAERS)
Peer-Reviewed Journal
ISSN: 2349-6495(P) | 2456-1908(O)
Vol-9, Issue-7; July, 2022
Journal Home Page Available: https://ijaers.com/
Article DOI: https://dx.doi.org/10.22161/ijaers.97.2

Validation of a post-cracking law in tensile for a sustainable UHPFRC using fracture energy and finite element method

Rosangel Rojas Aguero[1], Jose Rafael Yepez Aguirre[1], Américo Campos Filho[2], Alexandre Rodrigues Pacheco[2]

[1]Engineering School, Federal University of Rio Grande, Brazil
Email: r.rojas@furg.br, j.yepez@furg.br
[2] Engineering School, Federal University of Rio Grande do Sul, Brazil
Email : americo.campos.filho@gmail.com, apacheco@ufrgs.br

Received: 03 Jun 2022,
Received in revised form: 27 Jun 2022,
Accepted: 02 July 2022,
Available online: 08 July 2022
©2022 The Author(s). Published by AI Publication. This is an open access article under the CC BY license (https://creativecommons.org/licenses/by/4.0/).

***Keywords*— experimental tensile test, finite element method, fracture energy, inverse analysis, UHPFRC.**

***Abstract*—*Ultra-high performance fiber reinforced concrete (UHPFRC) is an advanced composite material characterized by compressive and tensile strengths above 150MPa and 7MPa, respectively. Initially, an experimental procedure was used to characterize the tensile performance through bending tests, using beams with 1% and 2% content by volume of steel fibers. Three-point bending load arrangement notched prisms were used to determine the contribution of the fibers to reinforcing a cracked section. With that, the (F vs. ω) experimental curves were graphed, and from there, the analytic tensile curves (σ vs. ω) was obtained point by point by application of the inverse analysis procedure proposed by the AFGC. With the analytic curves, the fracture energy was calculated, following a procedure proposed by RILEM. Subsequently, the crack width was transformed into strain using a relationship that involves the characteristic length. The resulting analytical behavior law was used to carry out computational modeling applying the finite element method. Both the finite element method and the fracture energy were used to validate the procedures, comparing experimental and numerical results. Models and experiments showed good agreement and finally was determined the constitutive law for the UHPFRC in tension. It can be concluded from this study, therefore, that the post-cracking tensile behaviour of UHPFRC can be appropriately evaluated and validated through the applied analysis procedure in this research.*

I. INTRODUCTION

Ultra-High Performance Fiber Reinforced Concrete (UHPFRC) is an innovative material that can reach average compressive strengths at 28 days that surpass 150MPa (22ksi), with tensile strengths of 7MPa (1ksi), and 10MPa (1.5ksi) in bending. To obtain a mix with ultra-high-strength, Camacho E. [1] observes that the water amount not chemically combined with the cement in the hydration process to be the less as possible, minimizing porosity and its connectivities, and increasing strength and durability. Schmidt and Fehling [2], additionally, have indicated that the particle packing should be optimized by

using large amounts of superplasticizers, adjusting the mix workability with the presence of fibers.

Four principles that must be met to achieve ultra-high strength and durability in concrete: (i) a very low water/cement ratio, which in our case was 0.19, resulting in a very dense and strong structure, minimizing pore capillarity and preventing the transport of toxic gases and liquids into and through the concrete; (ii) high particle packing, this requirement was not fulfilled, in our case a simple grinding process was carried out.; (iii) the use of a large amount of superplasticizer, to adjust workability; (iv) the use of fibers to increase tensile strength, flexural strength, and shear strength and to make the concrete sufficiently ductile. By keeping such general design rules, it is possible to define UHPFRC mixes for the use in beams, which should continue to have a great deal of bending strength even after cracking. During the post-cracking behavior, the fibers, subjected to tensile, have a fundamental role, since, when appropriately oriented, they tend to prevent a fragile rupture due to their bridging action that sews both sides of cracks together.

Naaman and Reinhardt [3] came up with a classification for Reinforced Concrete Fiber (FRC) that can be applied to UHPFRC. They classify FRC accordingly to the inelastic behavior: (i) tensile strain hardening, where the maximum internal force in the cracked zone is larger than the limiting elastic internal force, and (ii) tensile strain softening, where the limiting elastic force is larger than the maximum internal force. The recommendations made by the Association Française de Génie Civil AFGC [4] indicate that when UHPFRC is subjected to the tensile, it can present both behaviors just mentioned, as well as define an intermediate behavior, named as low strain hardening. In this work, UHPFRC beams with steel fiber content by volume of 1% and 2% were subjected to three-point bending tests in the lab. Their responses, in terms of load vs. deflection (F vs. δ), were recorded and showed herein graphically.

From there, the analytic tensile curves (σ vs. ω) was obtained point by point by application of the inverse analysis procedure proposed by the AFGC [4]. With the analytic curves, the fracture energy was calculated, following a procedure proposed by the International Union of Laboratories and Experts in Construction Materials, Systems and Structures, RILEM TC50 [5]. The crack width was transformed into strain using a relationship that involves the characteristic length. The resulting analytical behaviour law was used to carry out computational modeling applying the finite element method. The program ANSYS [6] was used to carry out computational modeling and obtain the analytical load vs. deflection curves. This program requires, as input data, the constitutive behavior of the material in compression and in tensile. The former can be specified with values directly obtained from the lab experiments, while the latter can be set with the Inverse Analysis. Both the finite element method and the fracture energy were used to validate the procedures, comparing experimental and numerical results, see Fig. 1.

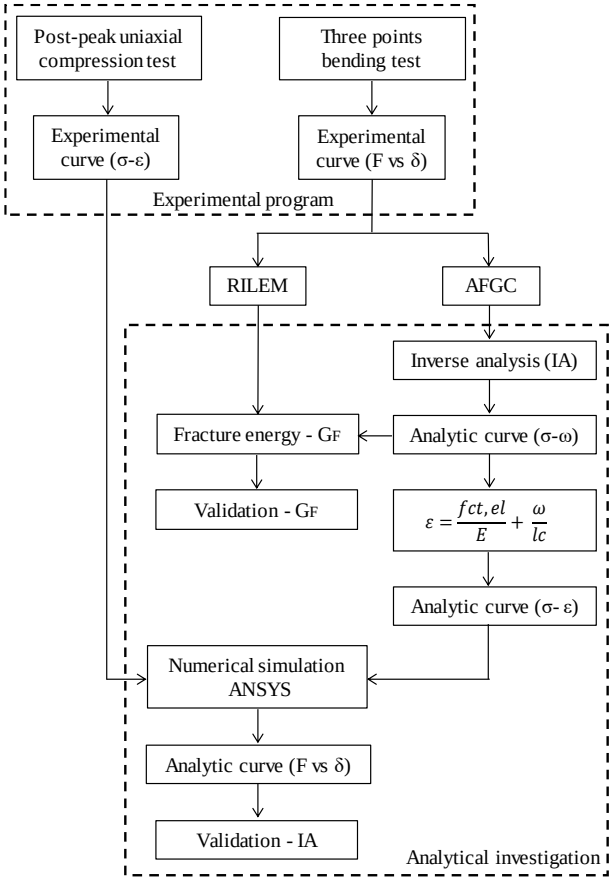

Fig. 1: Research scheme

II. EXPERIMENTAL PROGRAM

A practical strategy widely used in experimental programs to analyses the results of concrete resistance tests is the factorial arrangement, in which different treatments that are to be compared are defined. In the design of treatments, controllable factors, their levels and the combination between them are selected. The experimental design indicates the way in which the treatments are randomized and the way to control their natural variability.

The statistical tools indicated previously were used to define the UHPFRC mixture design used in this study, which was part of a series of studies carried out as support to an invention patent. It was deposited with the National Institute of Industrial Property (INPI), see Rojas et al. [7]. Also, those developments can be consulted in more detail in Rojas R. [8], it explains the extensive experimental work carried out, the end result of which is the design of the mixture indicated in TABLE 1, allowing the

production of UHPFRC with a compressive strength greater than 150 MPa.

Table 1: UHPFRC mix design.

Material	kg/m³
Cement	955
GGBS	263
Silica Fume	119
Quartz powder	119
Fine sand	788
Superplasticizer	40
Water	185

2.1 Materials

The agglomerating materials used in the mixture are made up of:

– National cement type Portland CP V ARI with high initial resistance.

– Ground Granulated Blast Furnace Slag (GGBS) donated by the company ArcelorMittal Tubarão in the Brazilian state of Espirito Santo. In TABLE 2 we observe the chemical composition of the GGBS used in this research, including the ranges recommended in ACI 233R [9].

– Commercial silica fume (SF).

– Commercial quartz powder.

It has a single aggregate consisting of silica sand with a maximum grain size of 0.30 mm. A solution of polycarboxylate in an aqueous medium (Visco-Crete 3535) supplied by SIKA was used as a super-plasticizer additive, which adjusts the workability of the concrete and is mixed with normal water to be placed in the mix.

Table 2: Chemical composition of GGBS

Main chemical constituents	Percent by mass	Range ACI [25]
CaO	44.50%	32-45%
SiO2	30.22%	32-42%
Al2O3	7.92%	7-16%
Fe2O3	7.45%	0.1-1.5%
MnO	1.10%	0.2-1.0%
MgO	1.08%	5-15%

The fiber used is of the steel Dramix type, 13 mm long and 0.2 mm in diameter, in a volume equal to 1%. TABLE 1 shows the proportions of the mixture, in which 26% of the cement is replaced by sustainable materials (GGBS and SF) and 8% is replaced by quartz powder. The water/cement ratio is 0.19 and the water/binder ratio is 0.13.

2.2 Manufacturing the Mixture

A sustainable UHPFRC is produced in this research. It has a simple manufacturing process, without the need for elaborated and delayed grinding processes for the packaging of particles. Two types of industrial waste are included in the mixture, silica fume and mainly GGBS, the latter with a specific granulometric distribution indicated in the invention patent.

The materials are weighed and placed in a mixer in the following order: silica fume, cement, and blast furnace slag and silica sand. The dry materials are mixed for about 5 minutes before the superplasticizer previously mixed with the water is added to the mixture. Wet materials are mixed for about 10 minutes. Initially, a dry mix is observed until small spheres of material are formed; about 1 mm in diameter, these spheres get mixed together and progressively increase in diameter until they become a wet concrete paste.

It is observed how the material separates from the bottom of the mixer, acquiring the shape and consistency of a dense plastic mass, see Fig. 2. In this state, the mixture for the UHPFRC is considered ready and it is in this moment that the steel fibers are placed, mixing for approximately 2 minutes. After fabrication, the mixture is cast into the respective moulds, to be compacted on a vibrating table for 1 minute. The specimens are stored and covered with a plastic layer for 48 hours, after which they are placed in a thermal bathroom for 24 hours at a temperature of 60 °C and then at 90 °C for another 24 hours. They are then stored in a humid room at 23 ± 3 °C until the day of the test, avoiding in all cases thermal shock on the specimens.

Fig. 2: Mixture consistency.

2.3 Post-peak uniaxial compression test

From an experimental point of view, the compilation of consistent and accurate stress vs. strain data (σ-ε) is difficult. During the execution of the compression test,

when the first crack forms, the lateral strain exceeds its tensile capacity and the UHPFRC specimens (with fibers) behave elastically up to approximately 80 to 90% of their compressive strength.

After reaching the maximum resistance (fc), a progressive strain softening takes place in which the presence of fibers regulates the softening stage in a similar way as it happens in tensile, to later produce the ductile compression failure. Hassan et al. [10] found a post-peak measurement method, which consists of placing the circular rings with the LVDTs in the specimen only to measure the elastic state of the test. Additionally, two LVDTs are placed parallel to the specimen to measure the movement of the test machine head, allowing the recording of the post-peak stage. That method was used in this research to recording the post-peak behaviour of the UHPFRC subjected to uniaxial compression.

The uniaxial compression test was performed on specimens manufactured using steel moulds of 50mm diameter by 100mm height, containing a 1% fiber volume and following the criteria specified in the ABNT NBR7215 standard [11]. Twenty specimens, with 28 days of cure, were tested, applying monotonic displacement loading, using a 2000kN hydraulic machine at a rate of 0.5 mm/min. Previously, the superior and inferior face of each cylinder was levelled mechanically using a rectifier and its height is measured to verify the necessity of applying some correction factor in the resistance according to ABNT NBR5739 [12].

The values of the load vs. vertical displacement of each specimen are recorded. In the linear elastic part, the value of the strain is calculating by dividing the average displacements of the LVDTs by the initial length of measurement maintained by the circular rings. Later, with the appearance of the first crack, a multiple cracking phase occurs, in which the strain is obtained by dividing the average displacement of the external LVDTs (those that measure the displacement of the machine head) by the total height of the specimen. The stress in this stage was obtained by dividing the machine load by the cross-sectional area of the cylinder.

The characteristic compressive strength (fck) of the UHPFRC was calculated using the AFGC [4] recommendations, and the following considerations were taken into account:

– Apply the displacement control load.

– The specimen must exhibit a conical failure pattern.

– The average strength must be calculated on at least three specimens.

– The characteristic compressive strength value must be calculated by subtracting the Student's coefficient multiplied by the standard deviation from the average strength value.

2.4 Modulus of elasticity

The modulus of elasticity was calculated by measuring directly on the linear upward branch of the UHPFRC constituent curve, recorded for each of the uniaxial compression tests performed on cylindrical specimens.

A linear approximation is used with best fit σ-ε results between 0 and 80 % of the peak compression strength. The value of E_{cm} is then defined as the average modulus of elasticity of the UHPFRC or the average secant modulus of elasticity, calculated as the average of the twenty individual values obtained graphically.

2.5 Three points bending test

Three-point bending load arrangement notched prisms were used to determine the contribution of the fibers to reinforcing a cracked section. With that, the (F vs. ω) experimental curves were graphed. Ten beams (four with 1% of fiber content and six with 2%), were manufactured with the mix presented in TABLE 1 and with the dimensions of 10x10x40cm. The lab tests were carried out in a hydraulic universal testing machine with a capacity of 2000kN (450kip), after 28 days of curing and by applying displacements at a speed of 0.5mm/min (0.02in./min). All of them had a notch of 30mm in depth by 4mm in width at the bottom centre of their span length made with a circular saw.

A horizontal LVDT type sensor was placed to measure the opening of the notch (ω) and two vertical LVDTs, placed on each side of the beams, were used to measure their central deflection (δ), as illustrated in Fig. 3.

Fig. 3: LVDTs to measure ω and δ.

The sensors are attached by means of tabs glued, a fast-setting glue is used. The distance between tabs must be the same from one test to the next so that the initial

measurements can be corrected by subtracting the elastic strain.

The distance between tabs should be less than 4 or 5 cm and the stroke of the sensors must be at least 2 mm.

The test variability was controlled by using materials from the same batch and the same equipment to manufacture and test the specimens. The data results were digitally recorded for each test and graphically analyzed in load vs. deflection (F vs. δ) curves, as well as in load vs. crack width (F vs. ω) curves for each of the beams.

III. EXPERIMENTAL PROGRAM

The relationship between forces and strains can be directly determined when: the internal force in a structural element is uniaxial; the cross-section is known, and it is possible to directly measure the deformation on the element under the action of a load.

Using experimental data from uniaxial compression tests, σ vs. ε curves were obtained for the UHPFRC, which were then used as a part to input data for the computational modeling.

When the forces were in bending, the determination of the nonlinear strains was not direct and alternate analytical procedures had to be used in the calculations. The procedure to determine the constitutive law for the UHPFRC in tension, including the post-cracking response, followed the methodology by AFGC [4].

The tensile curve was obtained point by point by application of the Inverse Analysis, i.e., obtaining the σ vs. ε analytic curve from the F vs. ω experimental curve.

Both curves σ vs. ε in compression and in tension were introduced as input data for the computational modeling and then the F vs. δ analytical curve was obtained. Therefore, a graphical comparison between the experimental and the analytical behaviors for each of the specimens tested were carried out.

3.1 Inverse analysis

The process starts with the definition of a new coordinate system at the point where the first crack occurs. The notch opening value at that point is turned into the new origin, with the first point coinciding with the elastic limit.

The equilibrium is easily solved to find the internal force. From the first point (step i), the next points are calculated (steps i+1) by solving the equilibrium of the cracked section.

A complex nonlinear equation system is generated at each step and, therefore, the free software Máxima [13] was used as a mathematical tool to solve the equations.

After solving the equation system, the force at the point is calculated, i.e., in this case, the cohesive force. The process is repeated at each i+1 point until the curve of cohesive force versus notch opening is built (actually, the σc vs. ω curve). Then, the σc vs. ω curve is transformed into a σ vs. ε curve, which, according to AFGC [4], can be used to define a relation between ω and ε mainly based in a determination of the characteristic length (lc) see equation 1:

$$\varepsilon = \frac{fct,el}{E} + \frac{\omega}{lc} \quad (1)$$

where:

fct,el is the tensile strength of the concrete matrix;

E is the modulus of elasticity of the concrete matrix;

lc is the characteristic length; and

ω is the notch opening.

The characteristic length is measured at the location where cracking occurs and in the same direction of the bottom notch opening of the beam. In the case beams are subjected to three-point bending, the AFGC [4] defines the lc value as a function of the type of experimental behavior that is presented, i.e., the value depends upon the behavior as either of the strain softening or strain hardening types.

If the beam presents a strain softening type of behavior, the characteristic length is calculated with equation 2, while if presenting a strain hardening behavior, equation 3 is therefore used.

$$lc = \frac{2\,(h-a)}{3} \quad (2)$$

$$lc = \frac{E.\ G_F}{fst^2} \quad (3)$$

where:

fst is the direct tension strength;

a, h are the notch depth and the beam height, respectively; and

G_F is the fracture energy.

3.2 Finite element method (FEM)

The computational analysis was carried out with software ANSYS [6] and choosing its element SOLID185 to model the concrete in 3D.

After the concrete experiences a cracking phase, the internal forces are transmitted to the fibers, which then govern the behavior of the material.

The Multilinear Material Model used in this work (CAST) can approximate behavior laws both in compression and in tension. Fig. 4 describes the boundary conditions of the beam considered in the model.

The UHPFRC was simulated as a composed material with a law in compression that was obtained from experimental data and a law in tension from an Inverse Analysis that includes the material's post-cracking behavior.

SOLID185 is a 3D element that allows considerations to represent plasticity, hyperelasticity, large displacements, and large strains. It also allows simulations of quasi-incompressible elastoplastic materials and fully incompressible hyperelastic materials.

The element is defined by eight nodes with three degrees of freedom each (translations in x, y, and z directions), as shown in Fig. 4.

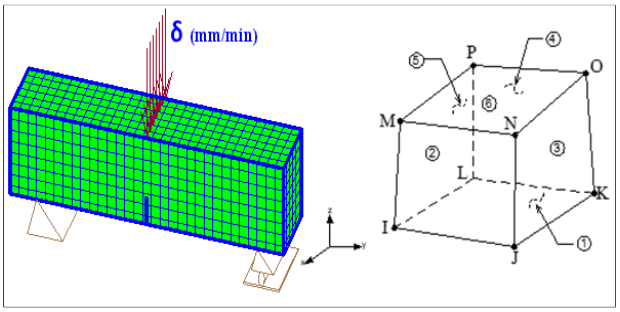

Fig. 4: Boundary element and element SOLID 185.

CAST is an elastic isotropic multilinear material with the same elastic behavior in compression and in tension, but with elastic limit and isotropic hardening behavior that can be different in each case. The behavior in tension uses the Rankine criterion, while the behavior in compression uses Von Mises.

The UHPFRC properties, such as its modulus of elasticity and its Poisson's coefficient, had to be known for the simulations. These values were maintained constant in each specimen that was modeled.

The behavior laws in tension and in compression were different in each specimen since those behaviors were drawn from the experimental tests and the results from the Inverse Analysis.

3.3 Forces in cracked section

Fig. 5 shows the cracked cross-section of a prismatic beam subjected to bending forces, and where two different regions can be easily identified.

Firstly, there is the zone without any cracking, which is the part of the section where the force distribution corresponds to a linear elastic behavior.

Secondly, there is the cracked zone, which is the part of the section where the force distribution directly depends on the effectively of the fibers inside the concrete matrix, which can be determined via Inverse Analysis.

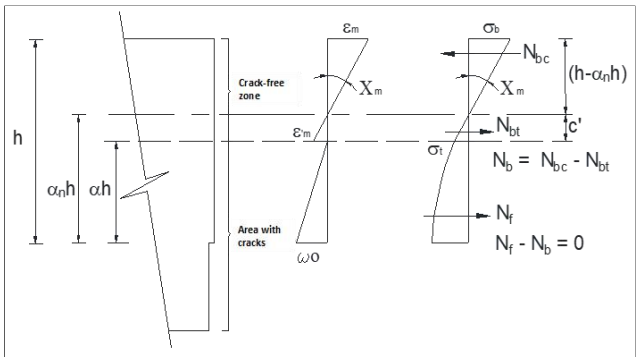

Fig. 5: Forces in the cracked section. AFGC [4] modified.

The force equilibrium in the section results in equations 4 to 8 with "b" identifying the contribution of the regions with cracks, while "f" identifies the cracked ones.

$$Nbc = \frac{1}{2}.\sigma b.c.b \quad (4)$$

$$Nbt = \frac{1}{2}.\sigma t.c'.b \quad (5)$$

$$Nb = Nbc + Nbt \quad (6)$$

$$M = Mb + Mf \quad (7)$$

$$N = Nb + Nf \quad (8)$$

The system of eight equations to solve is bound to equations 9 to 16, shown in the following.

$$Nb = \frac{1}{2}.E.Xm.b.h^2.[A^2 - B^2] \quad (9)$$

$$Nf_{i+1} = Nf_i.\ C.\ D + K.b.H.(1 - D) \quad (10)$$

$$Mb = \frac{1}{3}.E.Xm.b.h^3.[A^3 - B^3] + h.\alpha n.Nb \quad (11)$$

$$Mf_{i+1} = Mf_i.(C.D)^2 + K\ Nf_{i+1}.O - L.O^2\sigma f_{i+1} \quad (12)$$

$$N = Next = Nb + Nf \quad (13)$$

$$M = Mext = Mb + Mf \quad (14)$$

$$\sigma t = E.Xm.\ h.(\alpha n - \alpha) \quad (15)$$

$$\omega = \left[Xm + 2.\frac{M}{E.\ I}\right].\frac{2\ (\alpha.h)^2}{3} \quad (16)$$

where:

h.α is the relative length of the crack;

h.αn is the relative height of the neutral axis;

Xm is the curvature of the region without cracks;

b, h are the width and height of the beam cross-section, respectively;

I is the moment of inertia of the rectangular section; and the variables are:

$$A = 1 - \alpha_n; \quad B = \alpha - \alpha_n; \quad C = \frac{\alpha_{i+1}}{\alpha_i}; \quad D = \frac{\omega_i}{\omega_{i+1}}$$

$$H = \frac{\sigma f_i + \sigma f_{i+1}}{2}; \quad K = \alpha_{i+1}.h; \quad L = \frac{(\alpha_{i+1}.\ h)^2 .b}{2};$$

$$O = 1 - D$$

The equation system is solved for each point of the (σ vs. ω) curve by using the known experimental points (F, ω) and the parameters calculated in the previous step.

3.4 Validation using energy fracture

The area under the analytical (σ vs. ω) curve, which is obtained via the Inverse Analysis commented in the previous section, represents the fracture energy, GF, of the material. In the same form, the area under the experimental (F vs. δ) curve gives a measure of GF, calculated according to specifications given by RILEM TC50 [5].

The Fracture Energy can be found using the load-displacement data and the equation 17. A graphical comparison is made between both behaviors and the fracture energy is then calculated for every specimen with 1% and 2% of fiber content.

$$G_F = \frac{W_f}{b.(h-a)} \qquad (17)$$

where:

W_f is the total area of the curve under the graphic of load versus deflection;

b is the thickness of the beam (mm);

h is the height (mm); and

a is the length of the notch made in the lower center of the beam.

3.5 Validation using finite element method

The law of behavior in compression is obtained from the experimental data, and the law of behavior in tensile is obtained by inverse analysis.

The numerical simulation of the flexural test is performed using these behavior curves as input data. An analytical load-displacement curve is obtained for each of the specimens. Then this analytical curve is compared with the response obtained experimentally, as initially indicated in Fig. 1.

The approximation between the analytical and experimental curves, indicated above, is a measure adopted in this investigation to validate the inverse analysis. With this, it is possible to verify the effectiveness of the methodology proposed by the French standard in the AFGC [4], developed from the mechanical equilibrium of Fig. 5 and by equations 4 to 16.

IV. EXPERIMENTAL AND NUMERICAL RESULTS

4.1 Compressive strength and modulus of elasticity

Twenty cylinders measuring 5cm (2in.) in diameter and 10cm (4in.) in length were used for uniaxial compressive tests for the material with 1% of fibers. The compressive strength was calculated as the average for those twenty specimens, resulting in 151MPa (22ksi), as shown in TABLE 3 (fcm=151MPa). The standard deviation was 4.3MPa (0.7ksi).

Table 3: UHPFRC compressive strength and modulus of elasticity (1MPa=145psi).

Specimen	σ (MPa)	E (MPa)
1	154	50709
2	147	44504
3	146	46104
4	158	49551
5	150	48209
6	150	46780
7	146	47503
8	152	45802
9	153	44548
10	155	46556
11	144	43768
12	159	50799
13	147	47035
14	150	49184
15	150	49129
16	150	48193
17	146	45522
18	150	49293
19	152	49595
20	158	51374
Average:	151	47708

In each test, the σ-ε curve is obtained and the modulus of elasticity is calculated by a linear approximation between 5% and 80% of the compressive strength, which averaged 47708MPa (6919ksi), as also shown in TABLE 3. The standard deviation was 2.2MPa (0.3ksi).

Fig. 6 shows behavior the average curve in uniaxial compression for the tested specimens. The maximum compressive stress (fcm) value occurs for a strain value equal to 0.0033. The characteristic resistance value (fck)

was 143.43MPa (20.8ksi) with a 95% probability of exceedance, obtained using the Student-fisher law.

Cylinders containing 2% of fibers were tested; in all cases, the results showed resistance values significantly lower than those manufactured with 1% of fibers and therefore were discarded. We presumed that reduction of strength was due to fiber agglomerations and the formation of internal voids.

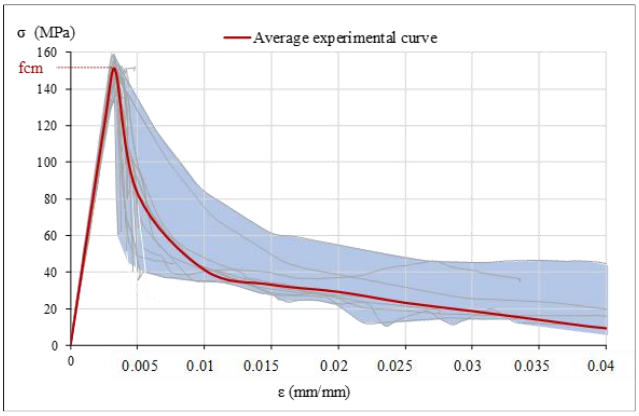

Fig. 6: UHPFRC compression constitutive behaviour.

The description in the previous paragraph meets the AFGC [4] recommendations, which proposes to characterize the compression behavior of UHPFRC according to the values of the characteristic compression strength and the modulus of elasticity.

4.2 Constitutive behaviour in tensile

Fig. 7 and Fig. 8 show (F vs. δ) curves for each of the tested beams, as well as the average curve and considering fiber content of 1% and 2%, respectively.

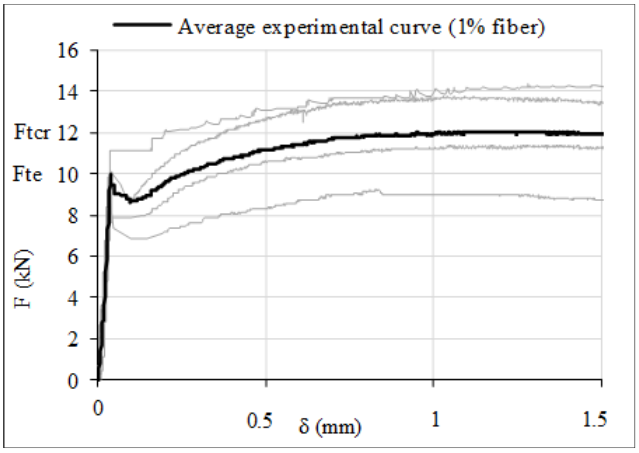

Fig. 7: Experimental curves for beams with 1% of fibers in bending (1kN=225lbf; 1mm=0,04in).

The area under each curve was calculated to determine the fracture energy according to RILEM TC50 [5].

The values of the elastic load, Fte; of the elastic strength in tension, σ; and of the deflection, δte; are presented in TABLE 4.

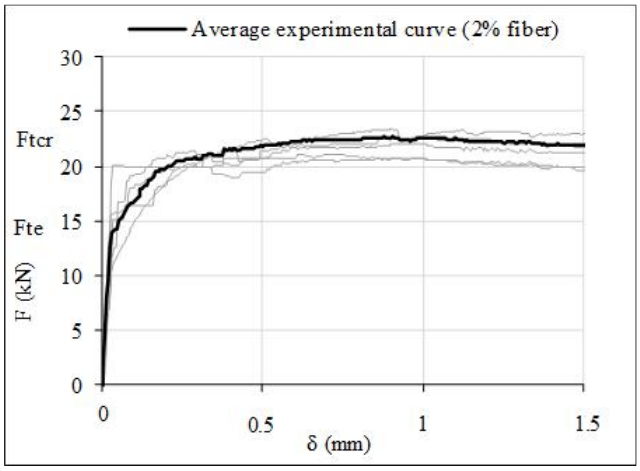

Fig. 8: Experimental curves for beams with 2% of fibers in bending (1kN=225lbf; 1mm=0,04in).

Table 4: UHPFRC elastic load and deflection, and strength in bending (1kN=225lbf; 1mm=0.04in; 1MPa=145psi)

	Fte (kN)		δte (mm)		σ (MPa)	
Specimen	1%	2%	1%	2%	1%	2%
CP-1	9.9	20.0	0.032	0.030	9.1	18.4
CP-2	10.0	15.1	0.039	0.024	9.2	18.5
CP-3	10.1	15.1	0.039	0.030	9.3	13.8
CP-4	10.6	10.3	0.037	0.020	9.7	9.5
CP-5		10.2		0.018		9.3
CP-6		10.3		0.021		9.4
Average	10.1	13.5	0.037	0.024	9.3	13.2

TABLE 5 presents the results obtained from the post-cracking behavior for the maximum load Ftcr and its corresponding deflection δtcr.

Table 5: UHPFRC inelastic load and deflection in bending (1kN=225lbf; 1mm=0.04in)

	Ftcr (kN)		δtcr (mm)	
Specimer	1%	2%	1%	2%
CP-1	9.2	21.0	0.83	0.81
CP-2	11.4	20.8	1.30	1.03
CP-3	13.8	22.5	1.04	1.08
CP-4	14.3	22.0	1.28	1.04
CP-5		23.4		0.91
CP-6		26.4		1.09
Average	12.2	22.7	1.11	0.99

Fig. 9 and Fig. 10 show (σ vs. ω) curves obtained from Inverse Analysis for each one of the beams, with fiber contents of 1% and 2%, respectively.

The area under each curve was calculated to determine the fracture energy.

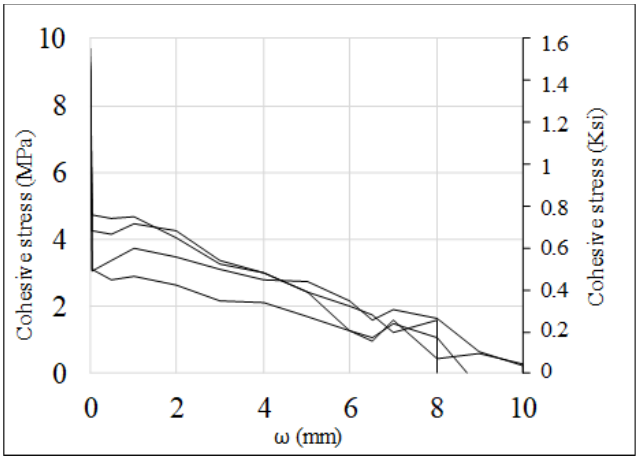

Fig. 9: Numerical (σ vs. ω) curves for beams with 1% of fibers in bending (1MPa = 145psi; 1mm = 0.04in).

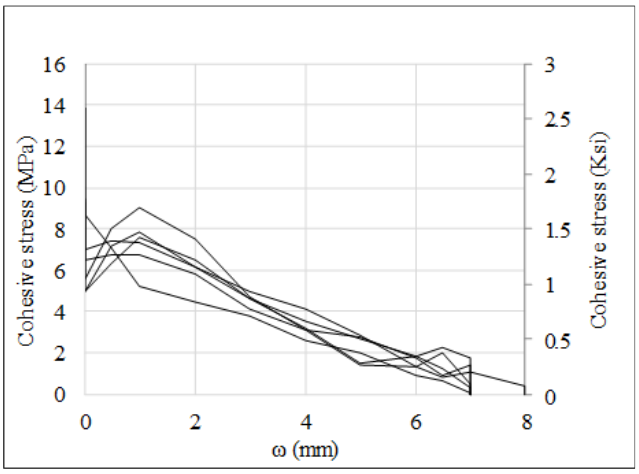

Fig. 10: Numerical (σ vs. ω) curves for beams with 2% of fibers in bending (1MPa = 145psi; 1mm = 0.04in).

It was calculated from the relations (F vs. δ) and (σ vs. ω) as is showed in TABLE 6 for each one of the tested specimens, where a good fit can be observed between the two averaged results.

Table 6: Fracture Energy (GF) for UHPFRC beams with 1% and 2% of fibers (1kJ/m2 = 0.0006BTU/in2).

	Fracture Energy (kJ/m²)			
	1% of fibers		2% of fibers	
	Inverse Analysis AFGC	RILEM TC50-FMC	Inverse Analysis AFGC	RILEM TC50-FMC
CP-1	16.91	11.66	26.53	23.76
CP-2	23.71	18.75	29.29	19.17
CP-3	23.70	15.42	29.19	23.10
CP-4	23.32	19.22	18.87	21.76
CP-5			32.49	32.40
CP-6			32.48	57.96
Average	21.91	16.26	26.67	24.04

Fig. 11 and Fig. 12 show (σ vs. ε) curves obtained from the transformation of ω into ε using equations 1 to 3, with fiber contents of 1% and 2%, respectively.

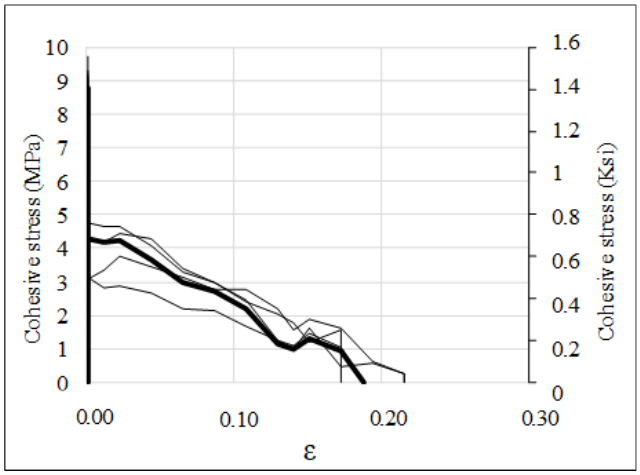

Fig. 11: Numerical σ vs. ε curves for beams with 1% of fibers in bending (1MPa = 145psi; 1mm/mm = 1in/in).

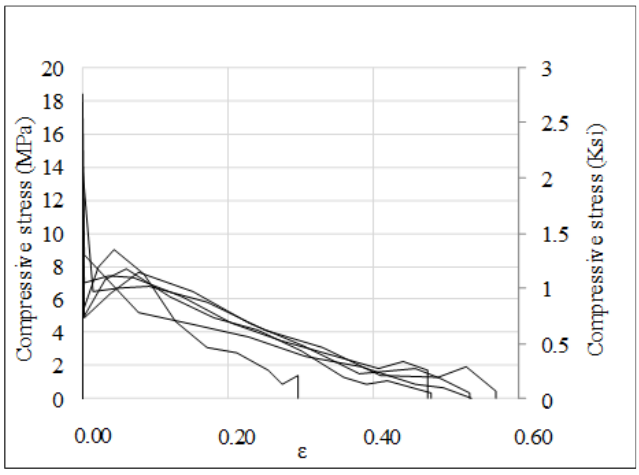

Fig. 12: Numerical σ vs. ε curves for beams with 2% of fibers in bending (1MPa = 145psi; 1mm/mm = 1in/in).

Fig. 13 and Fig. 14 show the results of computational modeling, with fiber contents of 1% and 2%, respectively. Models and experiments showed good agreement.

The behavior analytic curves obtained in this research showed a similar trend with the curves (F vs. δ) obtained by Denairé et al. [14] using inverse analysis. Similarly, Mezquida et al. [15] carried out inverse analysis methodologies, based on the closed-form non-linear hinge model, to define the material's behavior. They obtained a similar response to this research in both cases: when the UHPFRC exhibits strain-hardening constitutive stress-strain behavior and when it exhibits strain-softening behavior.

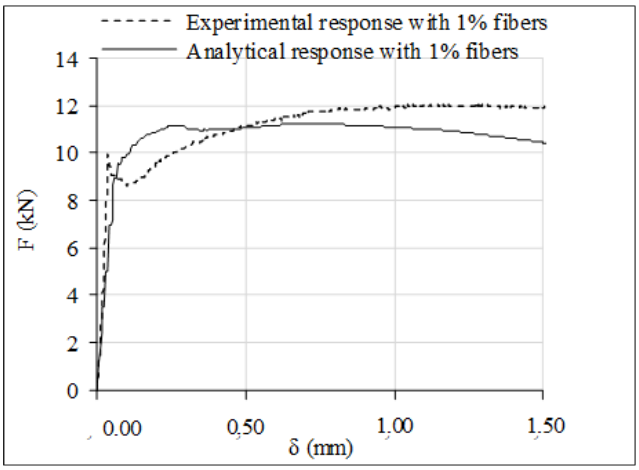

Fig. 13: Average response for 1% of fibers. Experimental vs. numerical (1kN = 225lbf; 1mm = 0.04in).

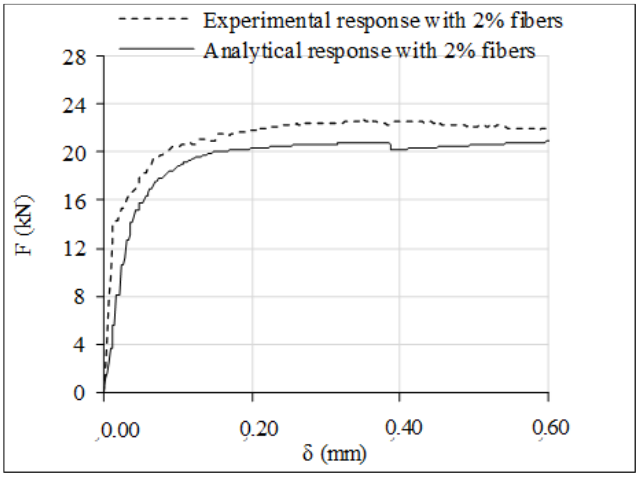

Fig. 14: Average response for 2% of fibers. Experimental vs. numerical (1kN = 225lbf; 1mm = 0.04in).

Also, Chanvillard and Rigaud [16] studied three points bend test on notched specimens and applied an inverse analysis to extract the tensile strength versus crack opening relationship. Again, the behavior curves showed a similar trend to the results in this research.

V. CONCLUSIONS

The results obtained from this investigation allow the following conclusions:

The computational modeling of UHPFRC beams can be satisfactorily carried out by considering the behavior of the composite material under a homogeneous premise. This can be accomplished with bending tests and the determination of behavior laws for the matrix with fibers in uniaxial compression and tension;

The constitutive laws for the UHPFRC material were experimentally and numerically determined for each of the beams considered. The σ vs. ε curves obtained in each case were considered as input data for the computational modeling carried out in Finite Elements in ANSYS. The results generated numerical F vs. δ curves that were compared with the ones experimentally obtained, showing a good fit between them;

The finite element SOLID185 used to model the matrix, together with the CAST material model used to simulate the behavior of the cracked section governed by fibers, were adequate to model the UHPFRC;

The Inverse Analysis procedure showed to be adequate to determine the behavior curve in tension of the considered beams made of UHPFRC, even considering the post-cracking response of the material;

The validation of the Inverse Analysis by means of calculating the fracture energy showed to be satisfactory for the beams with 2% of fiber content. The average value calculated from (σ vs. ω) numerical curves was 27 kJ/m2 (0.017BTU/in2), while the value obtained from the experimental (F vs. δ) curves was 24 kJ/m2 (0.015BTU/in2), i.e., a difference of roughly 10%.

ACKNOWLEDGMENTS

The authors acknowledge the financial support given by the Brazilian research agency CAPES as well as the personnel and equipment from the laboratories CEMACOM and LEME of the Graduate Program in Civil Engineering of UFRGS.

REFERENCES

[1] Camacho E. (2013). Dosage optimization and bolted connections for UHPFRC ties. Ph.D. Thesis, Valencia, Spain: Universitat Politècnica de València.

[2] Schmidt M. and Fehling E. (2005). Ultra-High-Performance Concrete: Research, Development, and Application in Europe. Digital format document: https://www.concrete.org

[3] Naaman A. and Reinhardt H. (2006). Proposed classification of HPFRC composites based on their tensile response. Journal Materials and Structures, n. 39, p. 547-5556. https://link.springer.com/article/10.1617/s11527-006-9103-2

[4] ASSOCIATION FRANÇAISE DE GENIE CIVIL. AFGC: Ultra High Performance Fiber Reinforced Concretes. Recommendations. AFGC, 2013.

[5] THE INTERNATIONAL UNION OF LABORATORIES AND EXPERTS IN CONSTRUCTION MATERIALS, SYSTEMS AND STRUCTURES. RILEM. TC50: Determination of Fracture Energy of Mortar and Concrete by means of three-point bend tests on notched beams. Materials and Structures Journals, v. 106, n. 18, p. 285-290, 1985. https://www.rilem.net/publication

[6] ANSYS Inc. Engineering Simulation Software. Version 19.2 Canonsburg, c2018.

[7] Rojas R., Korzenowski C., Yepez J., Beraldin R., Campos A., Maghous S. (2020). Composição de concreto, processo de obtenção de uma composição de concreto e usos de uma composição de concreto. Depositante: Universidade Federal do Rio Grande do Sul. Depósito: BR102020024167. Protocolo: 870200017039. Instituto Nacional de Propriedade Industrial (INPI).

[8] Rojas Aguero Rosangel. (2019) Estudio experimental y numérico de vigas usando Ultra-High Performance Reinforced Concrete-UHPFRC. PhD Thesis, Porto Alegre, RS, Brazil: Universidade Federal do Rio Grande do Sul.

[9] AMERICAN CONCRETE INSTITUTE. ACI 233R-95: Ground granulate blast-furnace slag cementitious constituent in concrete. ACI, 1995.

[10] Hassan A., Jones, S., Mahmud, G. (2012). Experimental test methods to determine the uniaxial tensile and compressive behavior of ultra-high performance fiber reinforced concrete (UHPFRC). Construction and Building Materials Journal, v. 37, p. 874-882.

[11] ASSOCIAÇÃO BRASILEIRA DE NORMAS TÉCNICAS. NBR 7215: Cimento Portland Determinação da Resistência à Compressão. Rio de Janeiro: ABNT, 1996.

[12] ASSOCIAÇÃO BRASILEIRA DE NORMAS TÉCNICAS. ABNT NBR 5739: Concreto. Ensaio de compressão de corpos de prova cilíndricos. Rio de Janeiro: ABNT, 2007.

[13] MAXIMA FREE SOFTWARE. wxMaxima version 17.10.1

[14] Denairé E., Sofia L., Brühwiler E. (2017). Characterization of the tensile response of strain hardening UHPFRC-Chillon Viaducts. AFGC-ACI-fib-RILEM Int. Symp. on UHPFRC, Montpellier, France.

[15] Mezquida E.; Navarro J. and Serna P. (2019). Numerical validations Numerical validation of a simplified inverse analysis method to characterize the tensile properties in strain-softening UHPFRC. Materials Science and Engineering, n. 596.

[16] Chanvillard G. and Rigaud S. (2003). Complete characterization of tensile proprieties of Ductal UHPFRC according to the french recommendations. In: HPFRCC, RILEM Proceedings Workshop, 2003, Ann Arbor, USA.